Journal of Geoscience and Environment Protection, 2025, 13(1), 32-50
https://www.scirp.org/journal/gep
ISSN Online: 2327-4344
ISSN Print: 2327-4336

Physical Origins of Spatial Pattern of Summer Extreme High Temperature Days over Northern Africa

Nestory Silvestry Mosha[1,2], Daniel Stephano Semgomba[2], Charles Yusuph Ntigwaza[2,3], Daniel Jonathan Masunga[2]

[1]State Key Laboratory of Climate System Prediction and Risk Management/Key Laboratory of Meteorological Disaster, Ministry of Education/Collaborative Innovation Center on Forecast and Evaluation of Meteorological Disasters, Nanjing University of Information Science and Technology, Nanjing, China
[2]Tanzania Meteorological Authority, Dodoma, Tanzania
[3]National Meteorological Training Centre, Kigoma, Tanzania
Email: nestorymosha@gmail.com, nestory.mosha@meteo.go.tz

How to cite this paper: Mosha, N. S., Semgomba, D. S., Ntigwaza, C. Y., & Masunga, D. J. (2025). Physical Origins of Spatial Patten of Summer Extreme High Temperature Days over Northern Africa. *Journal of Geoscience and Environment Protection, 13,* 32-50.
https://doi.org/10.4236/gep.2025.132004

Received: January 5, 2025
Accepted: February 14, 2025
Published: February 17, 2025

Abstract

In recent years, extreme high temperature events occurred more frequently in Northern Africa (NA) posing significant impacts on ecological systems and socioeconomic development. However, the physical origin of these extreme high temperatures remains unexplored. To address this issue, Empirical Orthogonal Function (EOF) analysis technics is employed to investigate the key physical factors influencing the spatial patterns of extreme high temperature days (EHDs) over NA. Three major modes of EHDs (EOF1, EOF2 and EOF3) accounting for 43%, 11% and 8% of the total variance were identified in this study. EOF1 features uniform distribution associated with positive geopotential heights and anticyclonic flows, while EOF2 is characterized by a meridional dipole pattern. Using reanalysis datasets, these modes are further linked to ocean – land – atmosphere interactions to reveal underlying physical mechanism. EOF1 is influenced by tropical and subtropical positive SSTA associated by mid tropospheric heights which triggers heat wave transport and subsidence. This mode is also influenced by weakening of west African monsoon system which suppresses moisture transport towards NA. EOF2 is influenced by combination of tropical Indian ocean and western Pacific wave trains leading subsidence over NA. EOF3 captures more the transient or regional scale influences on EHDs due to it weak association with large-scale teleconnections. Generally, this study classifies the factors influencing summer patterns of EHDs over NA as 1) tropical and subtropical SST warming, 2) decaying of Monsoon circulation, and 3) Strengthened upper-level subsidence. Gaining an

understanding of these processes is essential for improving climate prediction and setting strategies for early warning and mitigation of the impacts from extreme heat events.

Keywords

Extremely-High-Temperature Days, Interannual Variability, Empirical Orthogonal Function, Northern Africa

1. Introduction

In recent decades, occurrences of extreme high temperature events over various regions of the world have been increasing along with global warming (Lau & Nath, 2012; Meehl et al., 2000). The future projection suggests that, at least once every 20 years more than 9.0% (about 700 million people) and 28.2% (about 2 billion people) of the population worldwide will be seriously exposed to extreme high temperatures in a 1.5˚C and 2˚C warming world respectively (Dosio et al., 2018). Extreme high temperatures (EHDs) mostly occurring during summer are known to pose significant impacts on human health, agriculture, infrastructure and natural ecosystems (Intergovernmental Panel on Climate Change (IPCC), 2023).

In Northern Africa (NA), high production in olives, wheat, barley, and citrus fruits, makes agriculture to be is one of major sectors contributing largely to regional GDP and employment of substantial number of populations (African Development Bank, 2018). However, this region suffers from increased occurrence and intensity of extreme high temperature days (EHDs) and incidences of severe heatwaves (Dembélé et al., 2018; Lelieveld et al., 2016). Persistent EHDs in this region leading to sustained dehydrated soils and wildfire risk, ultimately causing crop failure, and exacerbating heat related fatalities (Lelieveld et al., 2016). For instance, in April 2010, NA suffered from severe thermal waves, with high temperatures exceeding 40˚C lasting for more than 5 days (Largeron et al., 2020). Not only that but also the most recent extreme heat wave hit NA during summer 2023 breaking the historical records with new maximum temperatures of 49.0˚C and 50.4˚C at Tunisia and Morocco respectively(WMO, 2024). Furthermore, it is estimated that, about 118 million of extremely poor African communities will be exposed to extreme high temperatures by the year 2030, with adaptation costs estimated to range from 30 to 50 billion US$ per year (WMO, 2024). Thus, investigation of the physical mechanisms influencing EHDs over NA is of urgent need for improvement of early warning systems and mitigation strategies.

Understanding the physical origin of EHDs is the foundation for accurate medium- and long-term climate forecasts over NA. This is due to the fact that the current climate forecasting dynamical models have limited skill in predicting EHDs (Gao et al., 2018; Long et al., 2022). To improve their simulation skill sufficient knowledge on the precursors of EHDs is highly required, therefore,

exploring physical mechanisms of EHDs focusing on heat prone region of NA is of great concern.

Generally, various studies relate the frequency of occurrence and intensity of EHDs to effects of anomalous local high-pressure systems resulting in adiabatic heating due to subsidence motion and enhanced land surface heating by direct solar radiation due to decreased cloud cover (Ding et al., 2018). Persistence of anomalous high-pressure systems over NA could be liked by various local and distant physical factors. For example, upper-level westerly jet enhances occurrence the formation of blocking pattern leading to prolonged anticyclones (Francis & Vavrus, 2012; Wang et al., 2016). It is also highlighted that, breaking of Rossby wave influence anomalous high-pressure systems by creating stationary weather patterns (Screen & Simmonds, 2014). Moreover, the anomalous high-pressure systems which ultimately enhances EHD over the region has been associated by the influence of teleconnection patterns, including circum-global teleconnection (Ding & Wang, 2005), North Atlantic Oscillation-NAO (Sun & Wang, 2012) and Pacific decadal oscillation-PDO (Zhu et al., 2020). Warm sea surface temperatures anomalies (SSTA) over the tropical and North Atlantic may activate propagation of wave trains (Sun et al., 2014) resulting in enhanced anticyclones over NA, ultimately favoring the occurrence and intensity of EHDs over the region (Deng et al., 2019). Furthermore, reduced Arctic Sea ice volume also influences atmospheric circulation in the Northern Hemisphere, leading to strengthened anticyclones through teleconnection (Budikova et al., 2019; Zhang et al., 2020).

Significant efforts have been made to understand the future trend of extreme temperatures over NA. However, it remains a challenge to explore the physical mechanism behind them. Current studies focused on NA show that this region responds quickly to global warming (Patricola & Cook, 2010; Lelieveld et al., 2016), and that more heat waves can pose major challenges that have global repercussions on human health and ecosystems. For example, the river Nile basin, which is the reliable source of water to multiple states in Africa can be seriously degraded by prolonged heat stress leading to water scarcity (Chakilu et al., 2023; Taye et al., 2011). The changes in heat wave dynamics over NA could also impact global climate systems, like monsoons and the Saharan heat low (Biasutti, 2013). Moreover, increased dust storm frequencies due to heat-driven Sahara Desert can reduce air quality leading to respiratory diseases both over NA and distant regions through transboundary transport (Harr et al., 2024). Such circumstances drive the need to conduct this study, based on two key questions: 1) what are the major spatial patterns of summer EHDs over Northern Africa during past century? and 2) what are the key physical mechanisms influencing these pattens? Relying on these questions, the dominant spatial and temporal pattens of EHDs are examined using Empirical Orthogonal Function (EOF) analysis, and then the corresponding large-scale atmospheric circulation patterns are explored. The organization of this research paper is as follows. Section 2 explains the data and methods and

definitions, Section 3 provides description of the results, Section 4 provides discussion, linking the results to the physical mechanisms influencing EHDs. Finally, Section 5 concludes the study.

2. Data and Methodology

2.1. Datasets

To investigate spatial patterns of summer EHDs over NA, daily maximum air temperature and mean temperature records with horizontal resolution of 0.5˚ × 0.5˚ were derived from National Oceanic and Atmospheric Administration – NOAA (Kanamitsu et al., 2002). In this study, NA refers to the region of Africa located north of 10˚N latitude encompassing countries of Morocco, Algeria, Tunisia, Libya, Egypt, Mauritania, Mali, Niger, Burkina Faso, Eritrea, Western Sahara, Guinea, Senega, parts Sudan, Chad, Ethiopia and Nigeria. To diagnose the physical mechanism behind EHD patterns over this region, the following monthly mean datasets were employed; 1) Sea surface temperature (SST), surface air temperature at the height of 2 m, precipitation, mean sea level pressure (MSLP), geopotential heights and wind fields at multiple levels, all obtained ERA5 with horizontal resolution 0.25˚ × 0.25˚ (Dee et al., 2011; Hersbach et al., 2020). The study focuses on summer months of May, June to July (MJJ) for the period covering 35 years (1979 to 2013). This time frame was selected as a baseline for comparison in our broad ongoing research work. Maintaining a consistent period promotes the overall robustness and rationality of the results across several related investigations and enables relevant cross-study comparisons.

2.2. Definition and Methods

2.2.1. Definition of EHDs

To define the threshold of EHDs over Africa, percentile (relative) threshold approach was used (Alexander et al., 2006; Fischer & Schär, 2010). Due to significantly large domain, this method is preferred than absolute threshold (Hong et al., 2022) and accounts for regional differences (Long et al., 2022) across the continent, therefore ensuring that, the defined EHDs reflects the regional climate variability. In this study, the percentile threshold of the 95% is used, this definition involves sorting of all daily records of maximum temperature for a specified period (1979-2013) and determine the 95th percentile as the threshold for EHDs at each grid. Days with temperatures exceeding this threshold were considered as EHDs.

2.2.2. EOF Analysis

The study utilizes Empirical Orthogonal Function (EOF) analysis, as given by Equation (1), to simplify the complexity and discover the most significant patterns that account for EHD variations (Hannachi et al., 2007; Jolliffe & Cadima, 2016). EOF analysis is a common statistical tool used to identify dominant modes of spatial patterns in meteorological and oceanographic complex datasets. To ensure the leading modes are independent of other modes and capture significant variance

in the datasets, we applied the North test (North et al., 1982). The principal components (PCs) associated with EOFs provide clear interpretation on the variation of the dominant spatial patterns over time to deeper understand the underlying physical factors influencing the variability (Lorenz, 1956). To link the EOF modes to physical mechanisms, correlation maps were generated between the PCs of the leading EOF modes and the climate variables.

$$\Phi_{ij} = \sum_{k=1}^{m} \mu_{ki} T_{kj} \tag{1}$$

where by: $i = 1, \ldots, m$; $j = 1, \ldots, n$; Φ_{ij} represent i^{th} components of the random vector (j^{th}) for the centralized data, μ_{ki} are the components of the eigenvectors of the correlation matrix; and T_{kj} are the dependent-time functions of the k^{th} component (principal components, PCs). m and n represent the number of grids and the length of time series respectively.

2.2.3. Correlation Analysis and Student's T-Test

To explore the relationships between variables, we employed Pearson's correlation coefficient (r) as given by Equation (2). This statistical measure quantifies the strength and direction of the linear association between two continuous variables, ranging from −1 (perfect negative correlation) to +1 (perfect positive correlation), with 0 (zero) indicating no linear relationship. Correlation analysis was particularly useful in identifying the degree to which variability in one variable was associated with variability in another within our datasets. The significance of the correlation coefficients was tested at 95% confidence level to ensure that observed relationships were not due to random variation. We also utilized the student's t-test (Equation (3)), which statistical test commonly used for evaluating whether the variables are significantly correlated.

$$r_{xy} = \frac{\sum_{i=1}^{N}(x_i - \bar{x})(y_i - \bar{y})}{\sqrt{\sum_{i=1}^{N}(x_i - \bar{x})^2}\sqrt{\sum_{i=1}^{N}(y_i - \bar{y})^2}} \tag{2}$$

$$t = \frac{r_{xy} \times \sqrt{N-2}}{\sqrt{1 - r_{xy}}} \tag{3}$$

where r_{xy} stands for correlation between two variables x and y, N is the total number of observed events, t is the test statistic and $\bar{x}$ and $\bar{y}$ are mean values of x and y respectively.

3. Results

3.1. Climatology of EHDs over Africa

It can be observed from **Figure 1** that, 95$^{\text{th}}$ percentile exhibit latitudinal gradient with highest threshold (exceeding 40˚C) in NA. This indicates that NA has more frequent and severely extremely high temperatures than other regions of Africa, reflecting the effects of semi-arid and arid regions surrounding it. Significantly, the 95$^{\text{th}}$ percentile decreases southwards from latitude 10˚N towards the central

and southern parts of Africa, reaching cooler temperatures below 25˚C.

Figure 2 shows seasonal distribution of climatological mean EHDs over Africa, indicating that the 95th percentile threshold captures seasonal distribution of EHDs effectively from January to December. During January to March (Figure 2(a) and Figure 2(c)) significant number of EHDs (reaching 11 days per month) appear to be located over the equatorial region between latitude 10˚S to 10˚N. Meanwhile, between April and August (Figure 2(d) and Figure 2(h)), substantial number of EHDs (reaching above 13 days per month) were located between latitude 10˚N to 40˚N (Tropical to Subtropical Zone). In the rest of the months i.e., September to December (Figure 2(i) and Figure 2(l)), EHDs reaching about 10 days per month were concentrated south of latitude 10˚ (Subtropical Southern Hemisphere).

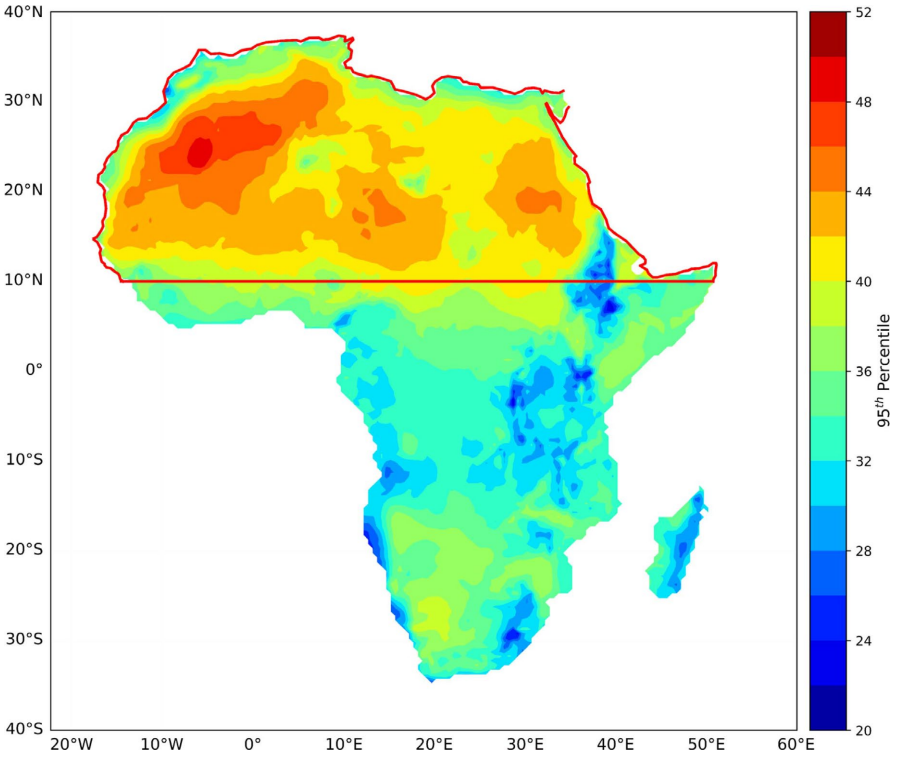

Figure 1. The distribution of the 95th percentile thresholds (˚C) defined for daily Maximum temperature over Africa during 1979-2013. The region enclosed by red line is the area experiencing highest percentile threshold (study area).

The spatial distribution of EHDs extracted at each grid over NA shows the highest number of EHDs in summer months of May, June and July (MJJ) with pick in June (Figure 3(a)). In this regard, MJJ was considered in this study as the main period of extremely high temperature days during summer months over NA (North of latitude 10˚N). Considering that, during MJJ, EHDs and mean temperature correlation over the large area of NA indicate substantial positive relationship at each grid, with domain average correlation coefficient (TCC) higher than 0.5 (Figure 3(b)). This relationship signifies that, evolution of both mean

temperature and EHDs at each grid point are influenced by similar atmospheric circulation patterns.

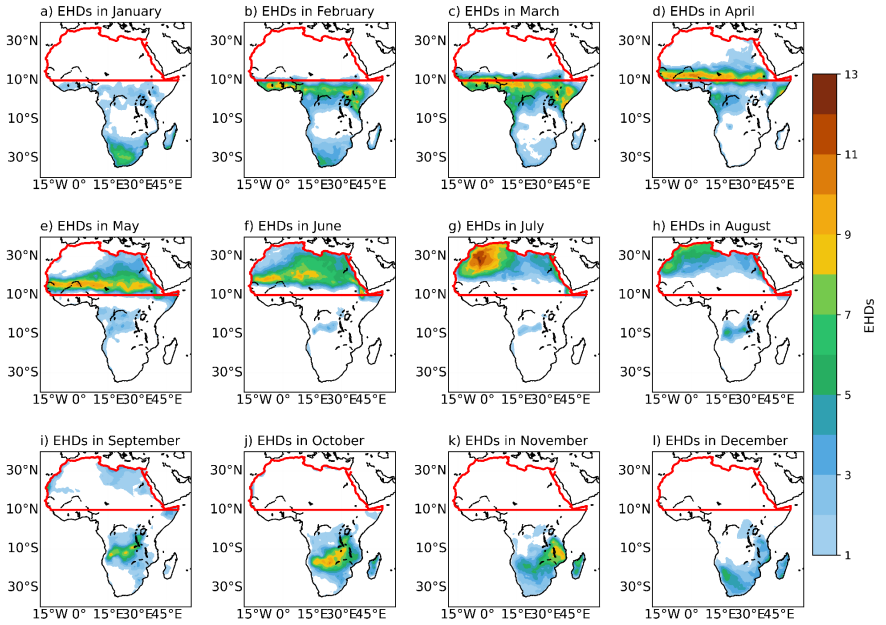

Figure 2. Climatological monthly mean EHDs (unit: days per month) over Africa in January to December (a)-(f) during 1979-2013 The region bounded by red line is the study domain.

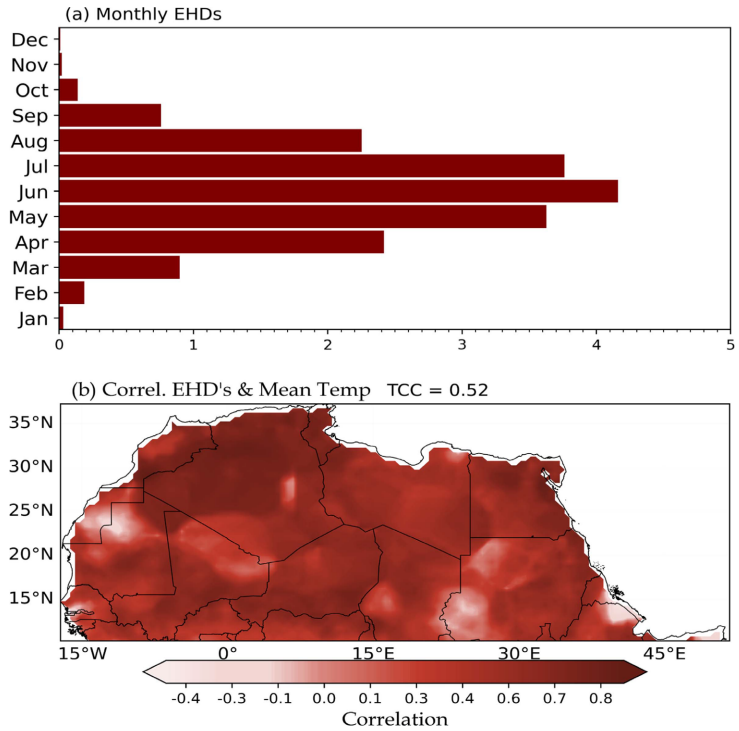

Figure 3. (a) Climatological monthly mean EHDs (unit: days per month) averaged over NA in January to December (b) Correlation between EHDs and mean temperature, over Northern Africa during 1979-2013.

3.2. Leading Modes of EHDs and Associated Anomalous Fields

In association with PCs time series, Figure 4 presents the EOF analysis intended for examining the drivers of summer EHD patterns over NA. The first three major EOF modes (EOF1, EOF2 and EOF3) of summer EHDs account for 43.0%, 11% and 8% of the total variance, respectively while the other modes account for the remaining small proportion of the total percentage variance (Figures 4(d)-(f), and Figure 5). The spatial loading (shaded regions), contours and wind vectors (Figures 4(a)-(c)) provides a clue to primary and secondary atmospheric circulation patterns influencing EHDs over NA. EOF1 mode (Figure 4(a)) captures strong influence over NA and demonstrates a homogeneous distribution of EHDs across the whole region. It corresponds to anomalous positive geopotential highs and anticyclonic flows at 850 hPa, which indicates intensifying extreme hot condition at the surface due to subsidence motion and advection of warm air from adjacent regions. The principal component (PC1) associated to this homogeneous mode (Figure 4(d)) shows inter-annual to decadal variation with a rising trend in the leading dominant mode, with negative values occurring before 1990 century and positive values after. This trend indicates that EHDs have become more common across NA in recent years as a result of climate change impacts, and that, there might be several underlying long term natural atmospheric processes influencing such extreme high temperatures (Chen & Tung, 2018).

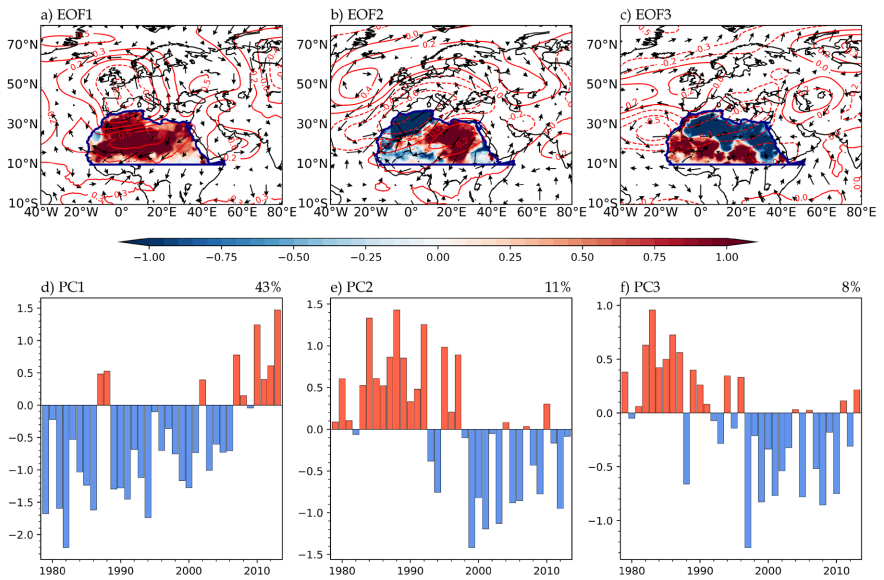

Figure 4. Spatial pattern (a), (b), (c) and Principal component (d), (e), (f) of the three major EOF modes of May– July EHDs in Northern Africa (area enclosed by blue line) during 1979-2013. Simultaneous coefficient of PC1, PC2 and PC3 with respect to geopotential height (red contours) and wind vectors (only corelation coeficient more than 0.30 are displayed) are shown in (a), (b) and (c).

EOF2 shows two regions with opposite temperature anomaly patterns (meridional dipole structure) over NA (Figure 4(b)). The patterns this EOF orient North

west to South east with negative loading to the closer to Mount Atlas and positive loading in the eastern part closer to River Nile basin. Such Meridional dipole spatial pattern suggests the presence of large-scale atmospheric circulation or surface conditions influencing extreme high temperatures over NA (Chen & Tung, 2018). The principal component (PC2) associated with EOF2 mode (**Figure 4(e)**) exhibits significant interannual to decadal fluctuations signify the influence of natural climate variability in the region. EOF3 pattern (**Figure 4(c)**) demonstrates a mixed region of positive and negative anomalies across NA, with localized hotspots of EHDs over the region between latitude 10˚N and 20˚N. Atmospheric circulation features associated to this EOF may suggest complex drivers for EHD events, such as localized convective activity or regional wind patterns. The principal components (PC3) associated with EOF3 mode (**Figure 4(f)**) exhibits significant interannual which also signify the influence of local or transient atmospheric patterns on EHDs. Generally, the independence existing between the PCs of the first three EOF modes is verified by North test (**Figure 5**) and suggests that the information captured by these initial EOF modes is distinct from that represented by other modes. Generally, it is evident that, EOF1, EOF2, EOF3 capture significant and unique sources of variation in the original data (Pavithra et al., 2019; Wold et al., 1987), therefore they can represent spatial variation of EHDs over NA.

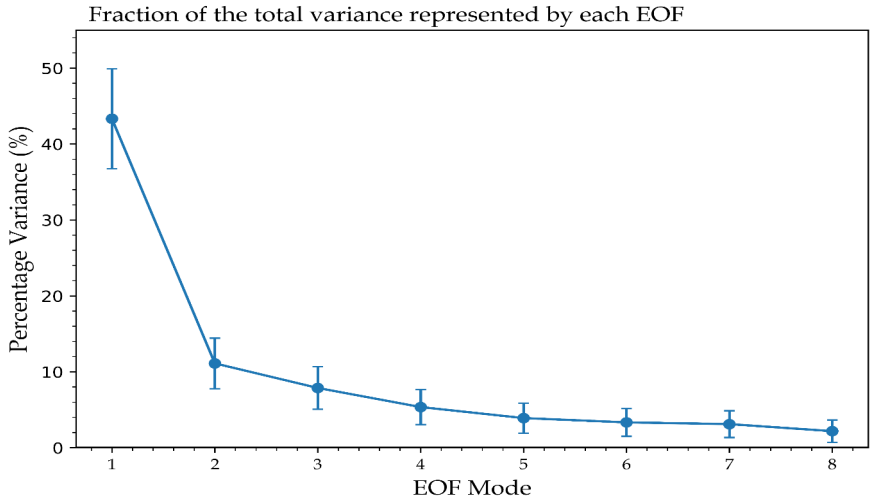

Figure 5. Percentage variances of the first eight EOF modes of MJJ EHDs and their standard deviation, during 1979 to 2013 over Northern Africa.

3.3. Underlying Physical Mechanism Influencing EHD Modes

To examine the underlying physical mechanisms of these EOF modes, we analyze the correlation between the PCs (PC1, PC2 and PC3) and various monthly mean meteorological variables during MJJ season. The variables include SST and 2-meter temperature (2 mT) and 500 hPa geopotential height denoted by Z (**Figure 6**), precipitation (PRE) and 850 hPa wind (UV) vectors, (**Figure 7**) and 200-hPa geopotential height and mean wave activity flux (WAF) (**Figure 8**). **Figure 6** and

Figure 7 which present the underlying patterns triggering the three modes of EHDs indicate that, EOF1 is characterized by extreme high-temperature days over NA. In this mode the positive anomalies of 2-meter air temperature coincide well with reduced rainfall across the entire region, this indicates that Precipitation and 2 m-temperature anomalies are well associated with intensification of EHDs (Figure 6(a) & Figure 7(a)).

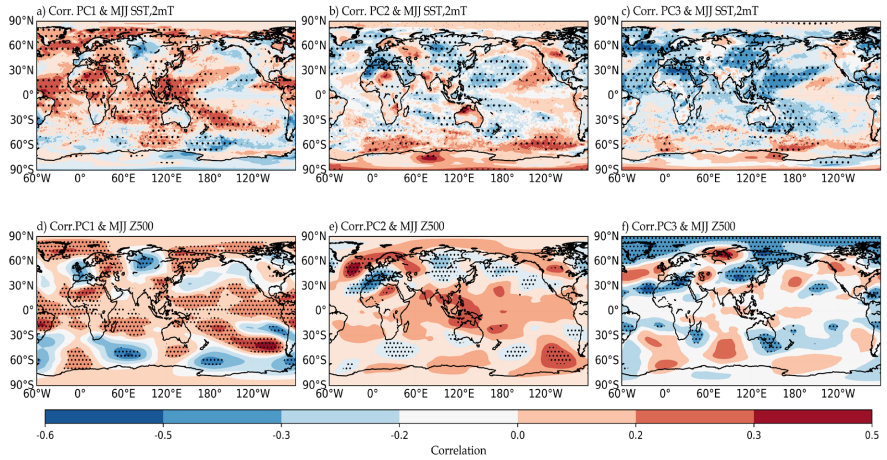

Figure 6. Correlation coefficient fields (May–July) between (a) PC1 and 2-m temperature (shading over land), SST (shading over ocean), (d) PCI and geopotential height at 500-hPa (shading), (b) PC2 and 2-m temperature (shading over land), SST (shading over ocean), (e) PC2 and geopotential height at 500-hPa (shading), (c) PC3 and 2-m temperature (shading over land), SST (shading over ocean), (f) PC3 and geopotential height at 500-hPa (shading) during 1979-2013. Dotted areas denote regions with correlation coefficients significant at 0.05 significance level.

Sea surface temperature anomaly (SSTA) on other hand reveal significant warming in the in the tropical and subtropical regions which includes the central Atlantic Ocean, Indian ocean and west pacific. Other SSTA warming is observed over Barents and Kara Sea (Figure 6(a)) which may result due to melting sea ice over this area. Significant cooling of SSTA is relatively experienced over North Pacific, western Europe experience relatively significant cooling (Figure 6(a)), This cooling is associated with low-pressure atmospheric pattern over these areas (Figure 6(d)). EOF2 is characterized by a weak dipole structure in the 2-meter temperature anomaly (Figure 6(b)) which corresponds with cooling of SSTA over western pacific, Indian ocean and Mediterranean region (Figure 6(b)). EOF3 is characterized by negative correlation scattered over North Atlantic and western pacific indicating the that, variability of this EOF may be influenced by localized SST anomalies. Moreover, the regions with negative (positive) summer mean 500-hPa geopotential heights anomalies (Figures 6(d)-(f)) match well with regions with low (higher) SSTAs and 2 m temperatures (Figures 6(a)-(c)) in both EOF modes.

In the correlation maps between PCs with precipitation and 850 hPa winds (Figure 7), strong negative precipitation is indicated over NA signifying dry

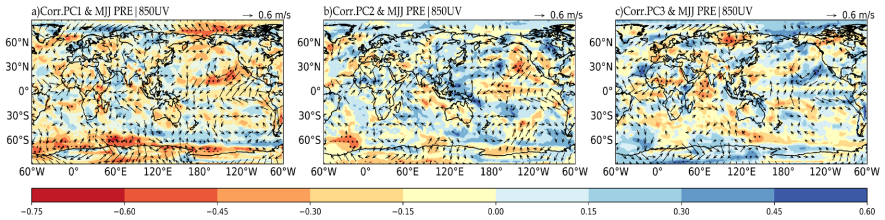

Figure 7. Correlation coefficient fields (MJJ) between (a) PC1, (b) PC2, (c) PC3 and (a and b) Precipitation (shading), 850-hPa wind (vector, only correlation coefficient exceeding 0.30 are shown) during 1979-2013. The *d*otted areas denote regions with correlation coefficients significant at 0.05 significance level.

condition over this region during MJJ season (**Figure 7(a)**), on other hand positive correlation appear over eastern Indian ocean, signifying increased convective activities over this region. Strengthening of easterly winds emanating from tropical Atlantic suggests weakening monsoon system into the NA (**Figure 8(a)**). Simultaneous correlation with PC2 (**Figure 8(b)**) indicates existence of dipole pattern with positive loading over western part of NA and negative loading over eastern part. This implies that EOF2 pattern over different parts of NA is associated with conflicting dry and wet conditions due transport of contrasting moisture properties.

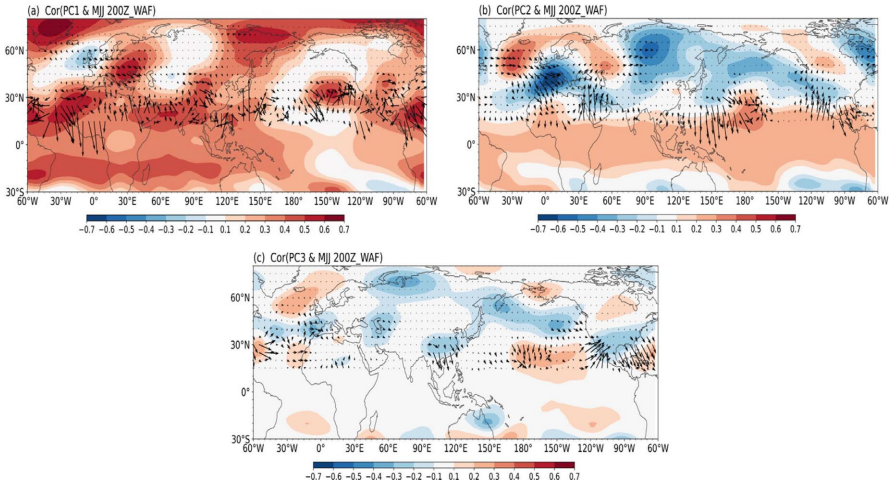

Figure 8. Correlation coefficient fields (MJJ) between (a) PC1, (b) PC2, (c) PC3 and Geopotential height at 200-hPa (shading), mean wave activity flux (WAF) at 200-hPa (unit: m^2s^{-2}) during 1979-2013.

The simultaneous correlation coefficients between PCs and meteorological fields at 200-hPa (i.e., geopotential height and mean wave activity flux (WAF)) shown in **Figures 8(a)-(c)** respectively revealed distinct pair of barotropic anticyclonic and cyclonic anomalies over north Atlantic, extending towards western Europe, Mediterranean and Eurasia. Specifically, the simultaneous correlation with PC1 (**Figure 8(a)**) features positive geopotential height anomaly appear over tropical to subtropical areas comprising NA, tropical North Atlantic and Eurasia,

while negative geopotentials are featured over mid latitude Atlantic and to the east of Mediterranean region. The flow direction indicated by of wind vectors (**Figure 8(a)**) suggests significant fluxes of Rossby waves from North Atlantic towards NA.

Moreover, barotropic anticyclonic and cyclonic anomaly pairs portrayed in the simultaneous correlation with PC2 (**Figure 8(b)**) are dominated by positive geopotential height anomaly positioned between North eastern Atlantic and western Europe and stretches further to subtropics of North Atlantic. On other hand, the negative correlations persist over the central Eurasia signifying existence of Upper tropospheric meridional dipole patterns. The direction of Wave activity (WAF) vectors signify flow of Rossby waves from North Eastern Atlantic to NA via Europe (**Figure 8(b)**). Furthermore, these paired anomalies play a significant role in the energy dissipation and transfer (Hurrell et al., 2003) and are well linked to their corresponding SST anomaly patterns displayed in **Figures 6(a)-(c)**. The direction flow from these barotropic systems is indicated by WAF vectors and suggests that their dynamics influence energy dissipation by westerly jets and Rossby waves towards NA. The simultaneous correlation of PC3 and 200 hPa geopotential height anomaly and WAF spread over mid latitude and tropical Atlantic, and central Pacific, while negative correlations appear over NA, Europe and Asia, indicating that, EOF3 (**Figure 8(c)**) is more influenced by localized atmospheric wave activity than EOF1 and EOF2.

4. Discussion

The mechanism behind the two major EOF modes of EHDs over NA is justified by the simultaneous correlation between PCs (PC1, PC2 and PC3) and land/ocean temperatures, 500 hPa geopotential heights, Precipitation overlayed by 850 hPa wind vectors and 200 hPa geopotential heights overlayed with WAF vectors. Both modes present a unique feature of variability over land, ocean and mid troposphere.

In the first EOF represented by PC1, it is clearly indicated that, EHD over NA is largely influenced warm SSTA persisting over the tropical and subtropical oceans (Atlantic, Indian and Pacific Oceans), and over Barents and Kara Sea (**Figure 6(a)**). Along with the variations in the mid-tropospheric circulation, this large-scale SSTA matches well with surface 2 mT existing over NA, indicating that SST warming over these oceans enhances atmospheric latent and sensible heat transport towards NA (**Figure 6(a)**) with major warming contribution being observed over the tropical Atlantic. With regards to Atlantic, this teleconnection relating large scale warming of SST over these regions is referred to as Atlantic Multidecade Variation (AMV) (Ting et al., 2011).

The significant warming of SSTA observed over the tropical western Pacific Ocean also influenced the first EOF mode of EHDs over NA. This suggests that EHDs over this region become more frequent and intense when the central part of Pacific Ocean experience warmer SSTs than average (specifically during El Niño), hence by weakening walker circulation and altering jet-streams (Wu et al.,

2021), this environment create high pressure systems over NA resulting to enhanced intense heatwaves. Furthermore, the significant warming of SSTA over Barents and Kara Sea (**Figure 6(a)**) suggests melting of sea ice at this region which discloses darker ocean surface to allow more warming of the ocean by solar radiation (Lien et al., 2024), and in turn influence the occurrence of MJJ EHDs over NA through teleconnection.

Positive 500 hPa geopotential heights experienced over the tropical and subtropical oceans (**Figure 6(c)**) are characterized by subsidence and stable atmosphere. Such condition suppresses convective activity by reducing cloud cover and cooling, to therefore raise the surface-air temperatures by radiation reaching land surface (Sultan & Janicot, 2003). The warming scenario agrees well with the persistence of warm SSTA over same locations (**Figure 6(a)**), which in turn strengthening anticyclonic activity to therefore enhancing heat wave fluxes towards the land surface (Lienert & Doblas-Reyes, 2013). The persisting of anticyclonic flow and warm temperatures over NA (**Figure 6(a)** and **Figure 6(c)**) is the clear demonstration of SSTA induced heat fluxes over land which ultimately led to the occurrence and intensification of EHDs over entire region.

The negative correlation in precipitation over NA (**Figure 7(a)**) indicates drier-than-normal conditions during MJJ which corresponds with the 2 mT observed over the region. The 850 hPa wind vectors show the northward shift of the low-level westerlies over the tropical Atlantic, with easterly anomalies across subtropics. Such patterns indicate a weakening of West African monsoon system (Giannini et al., 2008), which leads to decreased moisture transport towards NA leading to increased EHDs over the region. The dry conditions persisting over NA due to anomalous wind circulation provide evidence of the persistence of 500 hPa high-pressure systems which intensify EHDs as seen in **Figure 6(d)**.

The 200-hPa geopotential height anomalies overlayed by WAF (**Figure 8(a)**) indicates a strong upper-level ridge and stable atmosphere over NA which strengthens high pressure over the region by forcing subsidence which further leads to occurrence and intensification of EHDs. The NA ridge in both first and second EOF mode of EHDs is strengthened by strong barotropic cyclonic and anticyclonic pairs extending from Northeast of Atlantic Ocean, Europe, towards Mediterranean (**Figure 8(a)** and **Figure 8(b)**). The WAF vectors resulting from these barotropic pairs orient pointing southward towards NA suggesting that, the energy is being transported from mid latitudes towards NA by Rossby wave and westerly jet propagation hence leading to the intensification of EHDs. Meridional dipole structure which characterizes the second EOF mode of EHD over NA (**Figure 4(b)**, **Figure 6(b)** and **Figure 6(e)**), indicates that, NA is influenced by meridional wave trains associated by cooling of SSTA over western pacific and Indian oceans based in tropics. Convective activities over these tropical oceans are responsible for this cold SST and further triggers meridional wave trains by atmospheric convection and further subsidence over the continent (Huang & Yan, 1999; Zhu et al., 2020). This anomalous subsidence contributes to the occurrence and

intensification of EHDs over NA.

The third EOF (EOF3) which contribute 8% of the total variance depicts more localized and less regular atmospheric variability. The wave activity fluxes and anomalies in 200 hPa geopotential height (**Figure 8**) indicates weaker atmospheric teleconnection influences on EHD patterns compared to EOF1 and EOF2. This mode mainly affects precipitation and circulation over the western regions of NA and Mediterranean, with some localized increases in precipitation and moisture transport from the Atlantic. The weaker links with large-scale atmospheric dynamics would thus appear to indicate that EOF3 captures more the transient or regional-scale influences on EHDs.

Simultaneous correlation of principal components with SSTA, geopotential heights at 500 hPa and 200 hPa, precipitation and lower tropospheric winds provides clear differences in the three EOF patterns EOF1 is strongly associated with tropical and subtropical SSTA warming and inhibition of monsoonal flows, signifying that, tropical Atlantic SSTA variability is primarily important in the evolution of EHDs over NA. The second EOF shows significant relation to mid latitude dynamics pointing out of Atlantic, western Europe and Eurasian interaction due to existence of strong barotropic cyclonic and anticyclonic pairs responsible for drifting of Rossby waves towards NA. On other hand the PC of the third EOF demonstrate being weaker in large-scale teleconnections, it in most cases captures local dynamics.

5. Conclusion

To investigate the physical mechanisms influencing the spatial patterns of EHDs over NA during summer, the EOF analysis was used as a fundamental statistical tool to identify dominant modes of spatial pattens of EHDs. The focus was made on the first three EOF modes which account for 43%, 11% and 8% of the total variance respectively.

The first EOF, which shows a homogeneous distribution of EHDs, is associated with positive geopotential heights and anticyclonic flows, indicating the rising trend in EHDs. This Mode is largely driven by tropical and subtropical positive SSTA which enhances the transport of latent and sensible heat towards NA. The associated positive 500 hPa geopotential heights intensify the occurrence of EHDs over the region through enhanced upper-level subsidence motion and reduced cloud cover. Intensification of EHDs in the region could also be triggered by weakening of west African monsoon system by suppressing moisture transport towards NA.

The second EOF mode which accounts for 11% of the total variance presents a meridional dipole pattern, indicating the influence of EHDs by other external factors. This Mode is influenced by combination of tropical Indian ocean and western Pacific wave trains which make subsidence over NA leading to high pressure and ultimately enhanced EHDs over the region. Strong barotropic anticyclonic/cyclonic pairs charactering both modes trigger energy transport by Rossby

waves towards NA leading to enhanced EHDs over the region. The third EOF which accounts for about 8% of the total variance captures more the transient or regional-scale influences on EHDs because it is associated with weaker in large-scale teleconnections. In general terms the mechanisms influencing EHDs over NA can be classified as 1) tropical and subtropical SST warming, 2) decayed Monsoon circulation, and 3) Strengthened upper-level subsidence. Gaining an understanding of these processes is essential for improving climate model forecasts and setting strategies for early warning and mitigation of the impacts from extreme heat events.

As EHDs are becoming more prevalent in NA due to climate change, 'Our findings have significant implications for improving climate predictions and early warning systems in NA. By identifying and linking the major modes of EHD variability (EOF1, EOF2 and EOF3) to specific ocean-land-atmosphere interactions, we provide key insights into the physical mechanisms driving extreme high-temperature events. For instance, the influence of tropical and subtropical SST warming, the weakening of the West African monsoon, and strengthened upper-level subsidence offer actionable pathways to enhance predictive models. Incorporating these mechanisms into existing climate models could improve the accuracy of early warnings and assist policymakers and stakeholders in mitigating the socio-economic and ecological impacts of extreme heat events. Furthermore, the potential impacts of climate change on EHDs in NA are significant. As global temperatures continue to rise, the observed mechanisms such as increased SST anomalies and altered monsoon circulation are likely to intensify, potentially leading to more frequent and severe EHDs. These findings emphasize the urgency of developing climate-resilient strategies to adapt to and mitigate the impacts of extreme heat in this region. However, it should be taken into account that, the present findings offer a starting point that can be developed further with the use of other data sources and simulation techniques.

Moreover, in the future, the predictability of the anomaly pattern of summer extreme high-temperature days over Northern Africa could be scientifically investigated in order to provide a more comprehensive understanding of the specific mechanisms influencing the occurrence and intensity of EHD over the region, to therefore improve long and short-term predictions and enhance early warning systems.

Acknowledgements

This study was supported by Ministry of Commerce of People's Republic of China. Mosha Nestory Silvestry thanks Prof. Juan Li for helpful discussions. Furthermore, we thank anonymous reviewers for their valuable comments.

Conflicts of Interest

The authors declare no conflicts of interest regarding the publication of this paper.

References

African Development Bank (2018). *African Economic Outlook 2018: North Africa*. https://www.afdb.org/fileadmin/uploads/afdb/Documents/Publications/2018AEO/African-Economic-Outlook-2018-North-Africa.pdf

Alexander, L. V., Zhang, X., Peterson, T. C., Caesar, J., Gleason, B., Klein Tank, A. M. G., Haylock, M., Collins, D., Trewin, B., Rahimzadeh, F., Tagipour, A., Rupa Kumar, K., Revadekar, J., Griffiths, G., Vincent, L., Stephenson, D. B., Burn, J., Aguilar, E., Brunet, M., Vazquez-Aguirre, J. L. et al. (2006). Global Observed Changes in Daily Climate Extremes of Temperature and Precipitation. *Journal of Geophysical Research: Atmospheres, 111,* D05109. https://doi.org/10.1029/2005jd006290

Biasutti, M. (2013). Forced Sahel Rainfall Trends in the CMIP5 Archive. *Journal of Geophysical Research: Atmospheres*, *118*, 1613-1623. https://doi.org/10.1002/jgrd.50206

Budikova, D., Ford, T. W., & Ballinger, T. J. (2019). United States Heat Wave Frequency and Arctic Ocean Marginal Sea Ice Variability. *Journal of Geophysical Research: Atmospheres, 124,* 6247-6264. https://doi.org/10.1029/2018JD029365

Chakilu, G. G., Sándor, S., & Zoltán, T. (2023). The Dynamics of Hydrological Extremes under the Highest Emission Climate Change Scenario in the Headwater Catchments of the Upper Blue Nile Basin, Ethiopia. *Water, 15,* Article No. 358. https://doi.org/10.3390/w15020358

Chen, X., & Tung, K.-K. (2018). Global-Mean Surface Temperature Variability: Space-Time Perspective from Rotated EOFs. *Climate Dynamics, 51,* 1719-1732. https://doi.org/10.1007/s00382-017-3979-0

Dee, D. P., Uppala, S. M., Simmons, A. J., Berrisford, P., Poli, P., Kobayashi, S., Andrae, U., Balmaseda, M. A., Balsamo, G., Bauer, P., Bechtold, P., Beljaars, A. C. M., van de Berg, L., Bidlot, J., Bormann, N., Delsol, C., Dragani, R., Fuentes, M., Geer, A. J., Vitart, F. et al. (2011). The ERA-Interim Reanalysis: Configuration and Performance of the Data Assimilation System. *Quarterly Journal of the Royal Meteorological Society, 137,* 553-597. https://doi.org/10.1002/qj.828

Dembélé, A., Ye, X., & Touré, A. (2018). *Analysis of Land Surface Temperature Change Based on MODIS Data, Case Study: Inner Delta of Niger*. https://doi.org/10.5194/nhess-2018-208

Deng, K., Yang, S., Ting, M., Zhao, P., & Wang, Z. (2019). Dominant Modes of China Summer Heat Waves Driven by Global Sea Surface Temperature and Atmospheric Internal Variability. *Journal of Climate, 32,* 3761-3775. https://doi.org/10.1175/JCLI-D-18-0256.1

Ding, Gao, H., & Li, W. (2018). Extreme High-Temperature Event in Southern China in 2016 and the Possible Role of Cross-Equatorial Flows. *International Journal of Climatology, 38,* 3579-3594.

Ding, Q. H., & Wang, B. (2005). Circumglobal Teleconnection in the Northern Hemisphere Summer. *Journal of Climate, 18,* 3483-3505. https://doi.org/10.1175/JCLI3473.1

Dosio, A., Mentaschi, L., Fischer, E. M., & Wyser, K. (2018). Extreme Heat Waves under 1.5 ˚C and 2 ˚C Global Warming. *Environmental Research Letters, 13,* Article ID: 054006. https://doi.org/10.1088/1748-9326/aab827

Fischer, E. M., & Schär, C. (2010). Consistent Geographical Patterns of Changes in High-Impact European Heatwaves. *Nature Geoscience, 3,* 398-403. https://doi.org/10.1038/ngeo866

Francis, J. A., & Vavrus, S. J. (2012). Evidence Linking Arctic Amplification to Extreme Weather in Mid-Latitudes. *Geophysical Research Letters*, *39,* L06801.

https://doi.org/10.1029/2012GL051000

Gao, M., Wang, B., Yang, J., & Dong, W. (2018). Are Peak Summer Sultry Heat Wave Days over the Yangtze-Huaihe River Basin Predictable? *Journal of Climate, 31,* 2185-2196. https://doi.org/10.1175/JCLI-D-17-0342.1

Giannini, A., Biasutti, M., Held, I. M., & Sobel, A. H. (2008). A Global Perspective on African Climate. *Climatic Change, 90,* 359-383. https://doi.org/10.1007/s10584-008-9396-y

Hannachi, A., Jolliffe, I. T., & Stephenson, D. B. (2007). Empirical Orthogonal Functions and Related Techniques in Atmospheric Science: A Review. *International Journal of Climatology, 27,* 1119-1152. https://doi.org/10.1002/joc.1499

Harr, B., Pu, B., & Jin, Q. (2024). The Emission, Transport, and Impacts of the Extreme Saharan Dust Storm of 2015. *Atmospheric Chemistry and Physics, 24,* 8625-8651. https://doi.org/10.5194/acp-24-8625-2024

Hersbach, H., Bell, B., Berrisford, P., Hirahara, S., Horányi, A., Muñoz-Sabater, J., Nicolas, J., Peubey, C., Radu, R., Schepers, D., Simmons, A., Soci, C., Abdalla, S., Abellan, X., Balsamo, G., Bechtold, P., Biavati, G., Bidlot, J., Bonavita, M., Thépaut, J. et al. (2020). The ERA5 Global Reanalysis. *Quarterly Journal of the Royal Meteorological Society, 146,* 1999-2049. https://doi.org/10.1002/qj.3803

Hong, H., Sun, J., & Wang, H. (2022). Variations in Summer Extreme High-Temperature Events over Northern Asia and the Possible Mechanisms. *Journal of Climate, 35,* 335-357. https://doi.org/10.1175/JCLI-D-21-0043.1

Huang, G., & Yan, Z. (1999). The East Asian Summer Monsoon Circulation Anomaly Index and Its Interannual Variations. *Chinese Science Bulletin, 44,* 1325-1329. https://doi.org/10.1007/BF02885855

Hurrell, J. W., Kushnir, Y., Ottersen, G., & Visbeck, M. (2003). *An Overview of the North Atlantic Oscillation. The North Atlantic Oscillation: Climatic Significance and Environmental Impact* (Vol. 134). Geophys. Monogr.

Intergovernmental Panel on Climate Change (IPCC) (2023). *Climate Change 2021—The Physical Science Basis*. Cambridge University Press. https://doi.org/10.1017/9781009157896

Jolliffe, I. T., & Cadima, J. (2016). Principal Component Analysis: A Review and Recent Developments. *Philosophical Transactions of the Royal Society A: Mathematical, Physical and Engineering Sciences, 374,* Article ID: 20150202. https://doi.org/10.1098/rsta.2015.0202

Kanamitsu, M., Ebisuzaki, W., Woollen, J., Yang, S. K., Hnilo, J. J., Fiorino, M., & Potter, G. L. (2002). NCEP-DOE AMIP-II Reanalysis (R-2). *Bulletin of the American Meteorological Society, 83,* 1631-1644.

Largeron, Y., Guichard, F., Roehrig, R., Couvreux, F., & Barbier, J. (2020). The April 2010 North African Heatwave: When the Water Vapor Greenhouse Effect Drives Nighttime Temperatures. *Climate Dynamics, 54,* 3879-3905. https://doi.org/10.1007/s00382-020-05204-7

Lau, N.-C., & Nath, M. J. (2012). A Model Study of Heat Waves over North America: Meteorological Aspects and Projections for the Twenty-First Century. *Journal of Climate, 25,* 4761-4784. https://doi.org/10.1175/JCLI-D-11-00575.1

Lelieveld, J., Proestos, Y., Hadjinicolaou, P., Tanarhte, M., Tyrlis, E., & Zittis, G. (2016). Strongly Increasing Heat Extremes in the Middle East and North Africa (MENA) in the 21st Century. *Climatic Change, 137,* 245-260. https://doi.org/10.1007/s10584-016-1665-6

Lien, V. S., Raj, R. P., & Chatterjee, S. (2024). Surface and Bottom Marine Heatwave Characteristics in the Barents Sea: A Model Study. *State of the Planet, 4,* 1-11. https://doi.org/10.5194/sp-4-osr8-8-2024

Lienert, F., & Doblas-Reyes, F. J. (2013). Decadal Prediction of Interannual Tropical and North Pacific Sea Surface Temperature. *Journal of Geophysical Research: Atmospheres, 118,* 5913-5922. https://doi.org/10.1002/jgrd.50469

Long, Y., Li, J., Zhu, Z., & Zhang, J. (2022). Predictability of the Anomaly Pattern of Summer Extreme High-Temperature Days over Southern China. *Climate Dynamics, 59,* 1027-1041. https://doi.org/10.1007/s00382-022-06170-y

Lorenz, E. N. (1956). *Empirical Orthogonal Functions and Statistical Weather Prediction.* MIT Department of Meteorology Statistical Forecasting Project Scientific Rep.

Meehl, G. A., Zwiers, F., Evans, J., Knutson, T., Mearns, L., & Whetton, P. (2000). Trends in Extreme Weather and Climate Events: Issues Related to Modeling Extremes in Projections of Future Climate Change. *Bulletin of the American Meteorological Society, 81,* 427-436. https://doi.org/10.1175/1520-0477(2000)081<0427:TIEWAC>2.3.CO;2

North, G. R., Bell, T. L., Cahalan, R. F., & Moeng, F. J. (1982). Sampling Errors in the Estimation of Empirical Orthogonal Functions. *Monthly Weather Review, 110,* 699-706. https://doi.org/10.1175/1520-0493(1982)110<0699:SEITEO>2.0.CO;2

Patricola, C. M., & Cook, K. H. (2010). Northern African Climate at the End of the Twenty-First Century: An Integrated Application of Regional and Global Climate Models. *Climate Dynamics, 35,* 193-212. https://doi.org/10.1007/s00382-009-0623-7

Pavithra, N. L., Ashalatha, K. V., Megha, J., Manjunath, G. R., & Hanabar, S. (2019). Food Grain Production Index Using Principal Component Analysis in Karnataka State. *International Journal of Current Microbiology and Applied Sciences, 8,* 3138-3143. https://doi.org/10.20546/ijcmas.2019.801.335

Screen, J. A., & Simmonds, I. (2014). Amplified Mid-Latitude Planetary Waves Favour Particular Regional Weather Extremes. *Nature Climate Change, 4,* 704-709. https://doi.org/10.1038/nclimate2271

Sultan, B., & Janicot, S. (2003). The West African Monsoon Dynamics. Part II: The "Preonset" and "Onset" of the Summer Monsoon. *Journal of Climate*, *16*, 3407-3427. https://doi.org/10.1175/1520-0442(2003)016<3407:TWAMDP>2.0.CO;2

Sun, J. Q., & Wang, H. J. (2012). Changes of the Connection between the Summer North Atlantic Oscillation and the East Asian Summer Rainfall. *Journal of Geophysical Research: Atmospheres, 117,* D08110. https://doi.org/10.1029/2012JD017482

Sun, Y., Zhang, X., Zwiers, F. W., Song, L., Wan, H., Hu, T., Yin, H., & Ren, G. (2014). Rapid Increase in the Risk of Extreme Summer Heat in Eastern China. *Nature Climate Change, 4,* 1082-1085. https://doi.org/10.1038/nclimate2410

Taye, M. T., Ntegeka, V., Ogiramoi, N. P., & Willems, P. (2011). Assessment of Climate Change Impact on Hydrological Extremes in Two Source Regions of the Nile River Basin. *Hydrology and Earth System Sciences, 15,* 209-222. https://doi.org/10.5194/hess-15-209-2011

Ting, M., Kushnir, Y., Seager, R., & Li, C. (2011). Robust Features of Atlantic Multi-Decadal Variability and Its Climate Impacts. *Geophysical Research Letters, 38,* L17705. https://doi.org/10.1029/2011GL048712

Wang, W., Zhou, W., Li, X., Wang, X., & Wang, D. (2016). Synoptic-Scale Characteristics and Atmospheric Controls of Summer Heat Waves in China. *Climate Dynamics, 46,* 2923-2941. https://doi.org/10.1007/s00382-015-2741-8

WMO (2024). *State of the Climate in Africa 2023 (WMO-No. 1360).*

https://library.wmo.int/idurl/4/69000

Wold, S., Esbensen, K., & Geladi, P. (1987). Principal Component Analysis. *Chemometrics and Intelligent Laboratory Systems, 2,* 37-52. https://doi.org/10.1016/0169-7439(87)80084-9

Wu, M., Zhou, T., Li, C., Li, H., Chen, X., Wu, B., Zhang, W., & Zhang, L. (2021). A Very Likely Weakening of Pacific Walker Circulation in Constrained Near-Future Projections. *Nature Communications, 12,* Article No. 6502. https://doi.org/10.1038/s41467-021-26693-y

Zhang, R., Sun, C., Zhu, J., Zhang, R., & Li, W. (2020). Increased European Heat Waves in Recent Decades in Response to Shrinking Arctic Sea Ice and Eurasian Snow Cover. *NPJ Climate and Atmospheric Science*, *3*, Article No. 7. https://doi.org/10.1038/s41612-020-0110-8

Zhu, B., Sun, B., & Wang, H. (2020). Dominant Modes of Interannual Variability of Extreme High-Temperature Events in Eastern China during Summer and Associated Mechanisms. *International Journal of Climatology, 40,* 841-857. https://doi.org/10.1002/joc.6242